# Finite element modelling of the vibro-acoustic response in dielectric elastomer membranes

Giacomo Moretti[a], Gianluca Rizzello[a], Marco Fontana[b], and Stefan Seelecke[a]

[a]Department of Systems Engineering, Saarland University, Saarbrücken, Germany
[b]Institute of Mechanical Intelligence, Scuola Superiore Sant'Anna, Pisa, Italy

## ABSTRACT

This paper focuses on the characterisation of the vibroacoustic response of dielectric elastomer (DE) membranes. We set our attention on a circular DE membrane, deformed three-dimensionally and mounted in between fixed frames, which is able to generate sound with no need for any elastic or pneumatic biasing element.
We present a finite element model of the system entirely based on commercial software Comsol Multiphysics. The model combines: 1) a mechanical model of the DE membrane, which makes use of suitably defined energy functions that account for electro-elastic coupling; and 2) an acoustic model of the domain surrounding the DE. The model implements a bi-directional coupling between the DE and the acoustic domain. In particular, it accounts for the effect of the acoustic pressure loads applied on the DE membrane, which, given the small thickness and low density of the membrane, play a significant role in the system dynamics. We validate the model against experimental measurements of the DE surface velocity and the sound pressure level (SPL) in the surroundings of the membrane. Despite relying on strong simplifications in the geometry of the system and the viscous response of the material, the model is able to describe the main trends in the device frequency response, and how the SPL varies as a function of the mechanical pre-load and the voltage applied on the membrane.

**Keywords:** dielectric elastomer, loudspeaker, vibroacoustic, finite element, acoustics

## 1. INTRODUCTION

Dielectric elastomers (DEs) are polymeric multifunctional materials that, thanks to their large stretchability and dielectric behaviour, can be used to develop soft transducers.[1] Because of their low mass density, intrinsic softness, and high power density, they are regarded as a potentially game-changing technology in several applications, such as robotic actuation,[2] flexible electronics,[3] and mechanical energy harvesting.[4] Moreover, due to their ability to operate over a large frequency range, DEs are a candidate technology for the development of coil-free lightweight loudspeakers, in which a DE membrane plays the double role of acoustic diaphragm and actuator.[5]
Despite several proof-of-concept demonstrators of DE loudspeakers have been produced in the last few years,[6–9] only a few works have systematically investigated and modelled the vibroacoustic response of DE membranes and the parameters on which it depends.[10–13]

In this work, we present and validate a modelling framework for the vibroacoustic response of DE membranes, based on the finite element (FE) method. We focus our attention on a topology of DE actuator (DEA) that consists in a flat pre-stretched annular DE membrane, deformed out-of-plane (hence taking a truncated-cone-like shape) and held in place in between a couple of fixed frames. This layout is similar to a well known DEA layout, known as cone or circular out-of-plane DEA,[7,14,15] but it differs in that the membrane is blocked in the main actuation direction, and it can only vibrate perpendicularly to its own surface. In our previous works,[13,16] we proved that the high-frequency dynamics and acoustic response of conical DE membranes is governed by transverse vibrations, since the longitudinal degrees of freedom traditionally involved in the low-frequency operation of cone DEAs have a narrow passband and do not contribute in high-frequency dynamics.
We built a FE model of the system that combines an electro-elastic model of the DE membrane and a model of the acoustic domain. The DE is modelled as a membrane shell element (with no bending stiffness) with

Send correspondence to G.M.
E-mail: giacomo.moretti@imsl.uni-saarland.de

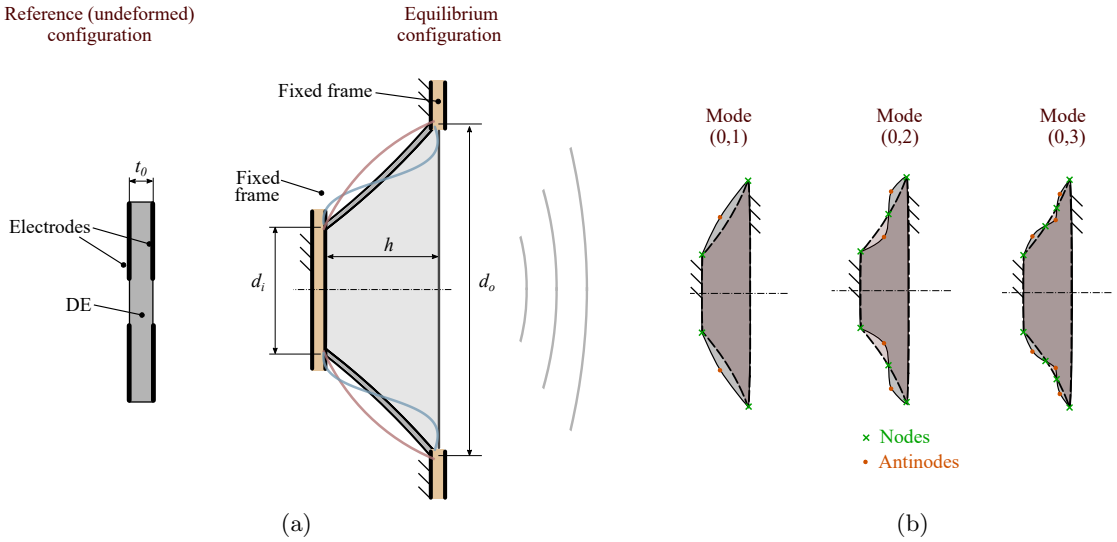


Figure 1: (a) Layout of the system: membrane in the flat unstretched configuration (left), and in the equilibrium working position (right), pre-stretched in-plane and conically deformed off-plane in between two fixed frames. (b) Examples of structural mode shapes of the DE membrane. Label $(0, n)$ denotes an axial-symmetrical mode (no circumferential nodes) with $n$ radial antinodes.

hyperelastic behaviour. Electrical coupling is implemented by assuming that the membrane behaves as a parallel-plate capacitor and formulating the strain energy function accordingly. The acoustic model is formulated in the frequency domain, and it is bidirectionally coupled to the DE model, so as to account for the contribution of acoustic pressure loads (namely, the acoustic impedance[17]) on the membrane dynamics. The FE model is implemented in the commercial program Comsol Multiphysics, using standard modules within the software, and making modifications to the default set of equations only to include the contribution of electro-elastic coupling. An experimental campaign is presented, in which the frequency response of a prototype is measured and used to validate the model in terms of the velocity profiles generated on the DE by high-frequency electrical excitation, as well as the resulting sound pressure level (SPL). The FE model is able to capture the general trend of the SPL, and it thus provides a convenient tool for the analysis and design of DE speakers, as it allows estimating the relevant eigenfrequencies of the system and the achievable SPL.
Compared to our previous work on conical DE membranes vibrations,[13] which just focused on an analysis of the vibration response, here we present a characterisation of the device SPL response. Compared to previous works on FE modelling of DE speakers,[11] the framework presented here relies on off-the-shelf codes, it has a relatively low implementation burden, and provides a convenient tool for the design of DE-based speakers.

The rest of the paper is structured as follows. Sect. 2 presents a description of the system layout and a formulation of the problem. Sect. 3 describes the assumptions and the structure of the FE model. Sect. 4 describes the experimental tests and provides a validation for the model. Sect. 5 draws the conclusions.

## 2. PROBLEM DESCRIPTION

The DE membrane layout under investigation is shown in Fig. 1a. The system consists of an initially flat membrane covered by compliant electrodes over an annular surface. The membrane is first equi-biaxially pre-stretched in plane, and then deformed off-plane and hanged to a couple of fixed frames, thus assuming the shape of a truncated conical shell. Whereas the central (circular) portion of the membrane is rigidly attached to the frame, the electrode-covered portion is free to vibrate and move transversally. We denote $t_0$ the initial membrane thickness (before pre-stretching), $d_o$ and $d_i$ the outer and inner diameters in correspondence of which the DE membrane is hanged to the frames, and $h$ the off-plane pre-load, i.e., the mounting axial distance between the inner and outer fixed diameters.
The DE membrane is subject to an initial deformation state similar to that present in a so-called cone DEA,[15,16]

with the difference that here the central portion of the actuator is blocked and cannot move in the longitudinal direction, whereas in cone DEAs this is connected to a free rigid disc attached to a compliant element (e.g., a spring), see Fig 1a. Whereas in cone DEAs voltage application leads to an expansion of the DE surface in the longitudinal direction (i.e., a linear stroke), in the layout of Fig 1a electrical excitation only induces transverse vibrations of the membrane, perpendicular to the electrodes deformed surface. Exciting the DE membrane with a high-frequency voltage waveform leads to complex frequency-dependent deformation patterns, described by the DE membrane eigenmodes. Examples of axial-symmetrical eigenmodes (with an increasingly large number of nodes) for the cone DE layout under investigation are shown in Fig. 1b. The main eigenmodes of the membrane recall those observed on flat pre-tensioned membranes with fixed rims, and are characterised by modal shapes whose natural frequency increases as the number of radial nodes and antinodes increases.[18]

High frequency excitation of the DE membrane leads to sound generation as a result of the excitation of the membrane structural modes.[16,19] In our previous work,[16] we presented a numerical investigation of a loudspeaker based on the cone DEA layout (i.e., a conically pre-loaded membrane with a floating rigid centre connected to a spring). In particular, we observed that, if the mass of the central rigid disc is much larger than the membrane mass, sound generation is entirely due to the membrane structural modes, whereas the longitudinal pumping motion of the rigid centre plays a minor role on the acoustic response. This observation was confirmed by measurements in a follow-up work.[19] There, we observed that the acoustic cut-in frequency of the speaker (i.e., the frequency above which the speaker can produce hearable sound) lies in proximity to the natural frequency of the first structural mode (denoted $(0,1)$ in Fig. 1b). In addition to that, we presented a systematic theoretical and experimental investigation of the structural vibrations in conical DE membranes, identifying the dependencies of the natural frequencies and their distribution on the geometrical parameters, the applied electric field bias, and the dynamic interactions between the DE membrane and the surrounding air domain.[13] Similar to previous works,[11] we observed that the DEA dynamics are highly influenced by acoustic loads, i.e., the pressure loads acting on the DE membrane surface as a result of its own vibrations, which result in an airborne mechanical impedance.[17,20] In particular, given the low thickness and mass density of the DE membrane, the added mass due to sound radiation is not negligible compared to the DE inertia, and it substantially affects the eigenfrequencies of the DE structural modes.
Because of such complex elasto-acoustic effects, the design of DE-based loudspeakers requires fully-coupled mathematical models, able to describe the bidirectional coupling between the air and the active membrane (i.e, how sound is generated from the DE motion, and how the DE membrane dynamics are influenced by the radiated sound).

We hereby investigate the vibroacoustic response of the system shown in Fig. 1a via a FE analysis, based on off-the-shelf software. Consistently with our previous observation that the dynamics of the conically-deformed DE membrane is dominated by axial-symmetrical modes,[13] we build a fully-coupled axial-symmetrical model of the DE membrane and the surrounding air domain, able to predict the resulting sound pressure level (SPL) generated by the DE, upon electrical excitation, at target receptor points.

## 3. FINITE ELEMENT MODEL

The FE model is implemented via off-the-shelf program Comsol Multiphysics,[21] by combining two of the software's in-built modules: Nonlinear Structural Material module and Acoustics module.

The DE structure is modelled as an axial-symmetrical membrane element, namely, bending stiffness is neglected, and no stress is assumed to act in the thickness direction. From the mechanical standpoint, the DE is treated as an incompressible material described by a generalised Mooney-Rivlin constitutive hyperelastic model.[22] Because the membrane thickness is orders of magnitude smaller than the DE radial dimensions, the electric field can be assumed perpendicular to the deformed electrodes surfaces (neglecting fringing effects). Based on this observation, the electrostatic problem is not explicitly solved for, and electro-elastic coupling is included in the model simply by modifying the default equation of the DE free energy density $\Psi$, and expressing it as follows:

$$\begin{aligned} &\Psi = \sum_{k=1}^{n} c_{k,0}(I_1-3)^k + \sum_{k=1}^{m} c_{0,k}(I_2-3)^k - \frac{\varepsilon}{2}\left(\frac{v}{t_0}\right)^2 \frac{J}{\lambda_3^2}, \text{ where} \\ &I_1 = \lambda_1^2+\lambda_2^2+\lambda_3^2,\ I_2 = \lambda_1^2\lambda_2^2+\lambda_2^2\lambda_3^2+\lambda_3^2\lambda_1^2,\ J=\lambda_1\lambda_2\lambda_3 \end{aligned} \tag{1}$$

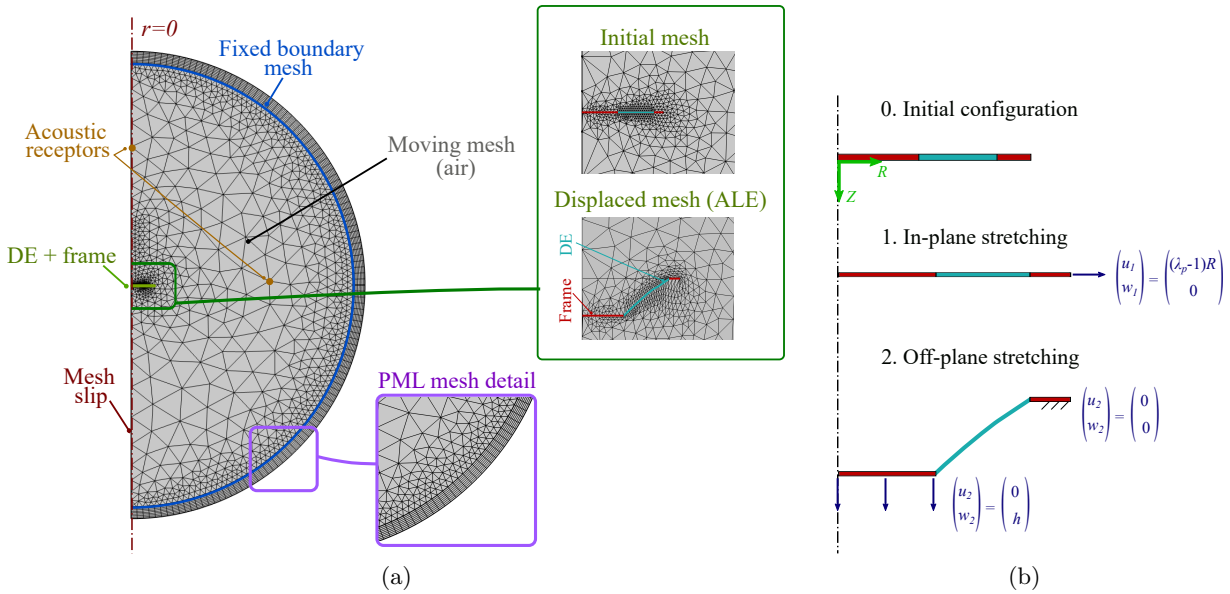


Figure 2: (a) Geometric model and mesh of the system. The insets show the detail of the PML mesh, and different configurations of the moving mesh, in the initial (unstretched) and the deformed configuration. (b) Phases of the static DE membrane pre-loading.

In Eq. (1), the first terms (summations) represent a multi-parameter Mooney-Rivlin energy density. In particular, coefficients $c_{k,0}$, $c_{0,k}$ are material constants; $J$ is the determinant of deformation gradient $\mathbf{F}$; $\lambda_1$, $\lambda_2$, $\lambda_3$ are the eigenvalues (under square root) of the right Cauchy-Green tensor, $\mathbf{C} = \mathbf{F}^T\mathbf{F}$, and they represent the principal stretches in the meridian, circumferential, and thickness direction respectively; $I_1$ and $I_2$ are the first and second principal invariants of $\mathbf{C}$. We used a version of the model with $n = 2$ and $m = 1$. The last term in the expression of $\Psi$ has the meaning of a generalised electrostatic potential energy (co-energy),[13,14,23] with $\varepsilon$ representing the DE permittivity, and $v$ the applied variable voltage. Eq. (1) is implemented by modifying the standard expression for the Mooney-Rivlin's energy density in the software, so as to include the last electrostatic coupling term. Incompressibility is dealt with by the software by means of a weak constraint ($\lambda_1\lambda_2\lambda_3 = 1$), which consistently introduces an auxiliary variable $p_w$ (Lagrange multiplier) used in the expression of the elastic component of the second Piola-Kirchhoff tensor $\mathbf{S}_{el}$ (describing the static stress on the DE), which thus reads as follows:

$$\mathbf{S}_{el} = -p_w J\mathbf{C}^{-1} + 2\frac{\partial\Psi}{\partial\mathbf{C}}, \tag{2}$$

where $\Psi$ is a function of $\mathbf{C}$ through the principal stretches.

Similar to Garnell et al.,[10] we model the material damping by means of a loss factor $\eta_s$ (rendering a dissipation that depends on the amplitude of the deformation, rather than the strain rate), and we hence express the total Piola-Kirchhoff tensor $\mathbf{S}$ (entering the equilibrium equations of the membrane) as follows in the frequency-domain:

$$\hat{\mathbf{S}} = (1 + i\eta_s)\hat{\mathbf{S}}_{el}, \tag{3}$$

where $i$ is the imaginary unit and $\hat{}$ denotes the frequency-domain representation of the associated variable.

For simplicity, the membrane and its holding frames (inner and outer frames) are modelled as a single hyperelastic element. Although the frames are held fixed (after pre-stretching) and play no role in the electro-elastic problem, they are included in the model so as to account for their interactions with the acoustic domain (e.g., sound reflection). No other elements (support structures, etc.) surrounding the DE sample are included in the model for simplicity.

The air domain surrounding the DE is modelled as a spherical volume with diameter equal to 20 times $d_o$, surrounded by a perfectly matched layer (PML) with thickness equal to $d_o/2$ (Fig. 2a). The PML has the

| Sample features | | Model assumptions | |
|---|---|---|---|
| Material | Elastosil 2030 mm | $c_{1,0}$ | 194 kPa |
| Thickness, $t_0$ | 100 $\mu$m | $c_{2,0}$ | 71 kPa |
| Pre-stretch, $\lambda_p$ | 1.2 | $c_{0,1}$ | -24 kPa |
| Outer diam., $d_o$ | 70 mm | $\varepsilon$ | $2.8 \cdot 8.9 \cdot 10^{-12}$ F/m |
| Inner diam., $d_i$ | 35 mm | $\eta_s$ | 0.15 |
| Outer frame diam. | 80 mm | DE density, $\rho$ | 1400 kg/m$^3$ |

Table 1: Features of the experimental prototype and parameters used in the model.

function of absorbing (without reflections) the sound waves leaving the acoustic domain, and it thus mimics an infinite open domain or an anechoic environment.
Within the acoustic domain, Helmholtz equation holds. In the frequency-domain, it is expressed as follows:

$$c_a^2 \nabla^2 \hat{p}_a + \omega^2 \hat{p}_a = 0, \tag{4}$$

where $c_a = 343$ m/s is the speed of sound in air, $\omega$ is the angular frequency variable, and $\hat{p}_a$ is the frequency-domain sound pressure $p_a$.

Whereas Eq. (4) is formulated in an Eulerian fashion, i.e., with reference to the pre-loaded deformed geometry of the DE, the nonlinear mechanics solver formulates the equilibrium equations for the DE membrane in a Lagrangian fashion, using the coordinates of the DE material points in the initial unstretched configurations as independent variables for the problem. The coupling between the two physics (structural mechanics and acoustics) is thus implemented using Comsol's moving mesh. This in fact provides a reformulation of the problem in an ALE fashion, creating a one-to-one mapping from the mesh coordinates to the deformed (pre-loaded) spatial configuration of the membrane. Specifically, here the air volume is treated as a deforming domain (with fixed outer boundary), where the nodes on the symmetry axis are free to slip tangentially, and the nodes on the membrane are prescribed displacements equal to the membrane static displacements (owing to the pre-load). A free triangular mesh is used (Fig. 2a), whose elements size varies depending on the proximity to the model components (DE, PML).

The simulation of the system is carried out in three steps:

- *Static pre-loading.* In this phase, the membrane is brought from its initial undeformed configuration to the deformed configuration shown in Fig. 1a. This step is further divided into two sub-steps (Fig. 2b): the membrane (with its support frame) is first equi-biaxially pre-stretched in-plane by a factor $\lambda_p$, and then its central portion is displaced off-plane by $h$. The off-plane displacement is applied in a progressive manner, by parametrically increasing the value of $h$ from 0 to the final target value. In this step, the membrane is subject to a constant bias voltage $v = V_b$.

- *Modal analysis.* In this step, the free eigenfrequencies and eigenmodes of the membrane are calculated.

- *Forced frequency-domain response.* In this step, a frequency domain analysis of the forced response of the system is performed. In this type of study, the response of the system is linearised in the neighbourhood of the equilibrium deformed configuration, and the response to a harmonic perturbation is computed. Here, a linear perturbation is applied to voltage $v$, which is expressed as:

  $$v = V_b + V_a \sin(\omega t), \tag{5}$$

  where $t$ is time, $\omega$ is the excitation frequency, $V_b$ and $V_a$ are a bias voltage and amplitude respectively. Waveform (5) for the voltage is coded into the user-defined expression of the electrostatic co-energy in Eq. (1) by means of Comsol's command `linper`.


(a) (b)

Figure 3: (a) Picture of the DE sample. (b) Sample and microphone installed inside an acoustic absorbing box.

## 4. EXPERIMENTAL CHARACTERISATION AND VALIDATION

### 4.1 Experimental characterisation

We built a system with the layout shown in Fig. 1a and the features listed in Tab. 1. The system consists in a silicone membrane made of a commercial film,[24] and it has screen-printed carbon-loaded silicone electrodes. The sample has dimensions and features similar to those of the samples used in our previous work.[13] The holding frames for the membrane were 3D printed in rigid plastic (see Fig. 3a). Although the mounting frames of the DE are not axial-symmetrical, the system is still representative of the symmetrical problem described in Fig. 1a and Sect. 3, as the effect of such asymmetries is not expected to significantly impact the membrane velocity profiles[13] and the sound pressure field at a sufficient distance from the membrane. Electrical driving was provided by a high-voltage amplifier Trek 609E-6. The specimen was installed in a custom-built acoustic chamber, with the walls made of a multi-layer sound absorbing foam, so as to limit reverberations from the surrounding environment. The box has dimensions of $110 \times 100 \times 80$ cm, and it has movable walls that can be opened so as to allow operations or optical measurements on the DE system. The acoustic response of the system was measured using microphone MM210 by Microtech Gefell (with conditioning module M33) located inside the acoustic box. In addition to that, we measured the velocity of a set of target points on the DE membrane (axial component) via laser vibrometer PSV-500 by Polytec. Data acquisition was performed using the proprietary data acquisition hardware and software of the vibrometer. For acoustic measurements, all the apertures of the box were kept closed, whereas for velocity measurements with the vibrometer, a frontal aperture was left open in between the laser sensors and the DE sample.

The off-plane displacement $h$ of the DE membrane is adjustable, therefore different tests with different values of bias deformation were carried out. Measurements were carried out by applying a sinusoidal sweep voltage signal on the DE membrane, and measuring its acoustic response or the velocity of the target points. Here, we used sweep signals with a frequency varying between 0 and 2 kHz in a timespan of 10 s, amplitude $V_a = 100$ V, and different values of the bias voltage $V_b$ between 1 and 3 kV.
The SPL is calculated from the acoustic pressure time-signal as follows:

$$SPL = 20 \log_{10} \left( \tilde{p}_a / p_0 \right), \tag{6}$$

where $p_0 = 20$ $\mu$Pa is the reference human hearing threshold, and $\tilde{p}_a$ is root-mean-square value of the acoustic pressure, calculated on a moving window of 5 ms.

### 4.2 Results and validation

The implementation of the FE model described in Sect. 3 relies on a mesh with approximately 2260 triangular elements in the acoustic domain, 960 quadrilateral elements in the PML, and 20 nodes on the membrane. A MUMPS solver is selected for all of the solutions steps, and Winslow smoothing method (with default parameters) is used for the moving mesh. The parameters listed in Tab. 1 were assumed for the model. The hyperelastic

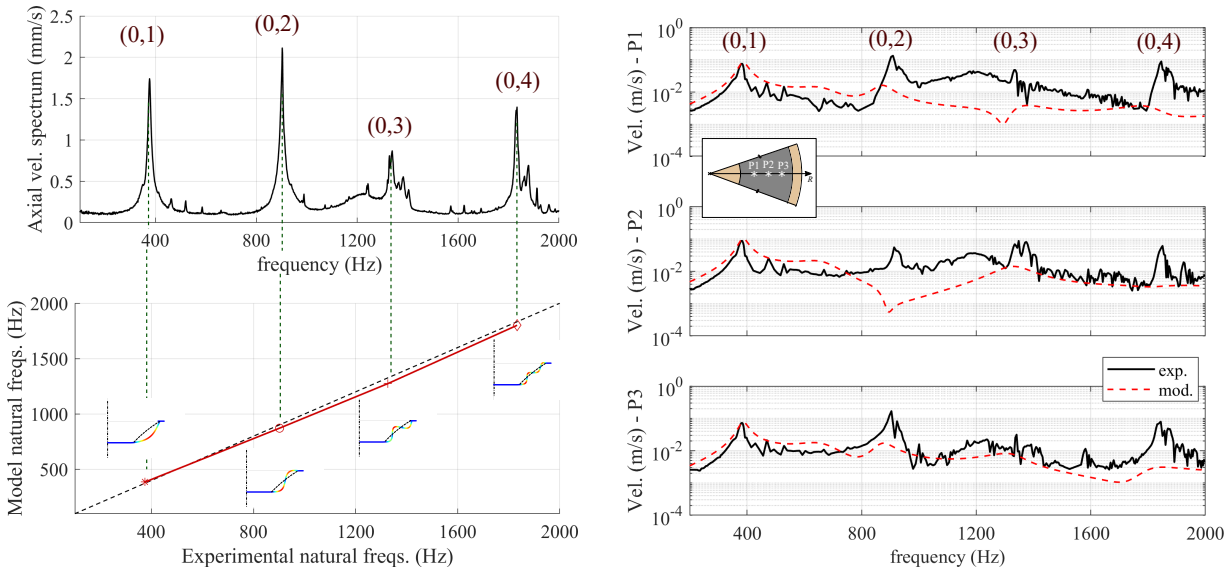


(a) (b)

Figure 4: (a) Experimental spectrum of the axial velocity, and comparison of the experimental and numerically predicted eigenfrequencies (for 4 symmetrical eigenmodes) of the system, for $h = 15$ mm and $V_b = 2$ kV. (b) Amplitude of the axial velocity of the DE membrane ($h = 15$ mm, $V_b = 2$ kV) as a function of frequency, at three different points, $P_1, P_2, P_3$, on the DE surface: FE model vs. experiment.

parameters were obtained from tensile measurements, whereas the density is estimated based on previous measurements of the samples mass.[13] It is worth remarking that the membrane's thickness $t_0$ used in the model is the nominal thickness of the dielectric layer, and the contribution of the electrodes mass/stiffness is kept into account indirectly via the chosen values of the density and the hyperelastic parameters.

We estimated the eigenmodes of the DE membrane experimentally, and compared them with the values obtained from the FE eigenfrequency analysis (neglecting, at this stage, the DE material damping). The experimental evaluation of the eigenfrequencies was done by exciting the DE with a periodic chirp with amplitude $V_a = 100$ V, and evaluating the Fast Fourier Transform (FFT) spectrum of the average axial velocity over a grid of points on the membrane (Fig. 4a). A grid of 80 points equally distributed over the DE surface was used for the purpose,[13] and the FFT spectrum was obtained via the vibrometer proprietary post-processing software. Since the DE's modal response is rather underdamped, the DE eigenfrequencies were evaluated from the frequencies of the peaks in the spectrum. With reference to a set of recognisable modes within the testing range (namely, modes $(0, 1)$ to $(0, 4)$, as defined in Fig. 1b), a comparison of the measured frequencies with those obtained from the FE model is shown in Fig. 4a. The dashed bisector line in the bottom plot represents a virtual perfect agreement between model and experiment, whereas the markers represent the actual measured/calculated eigenfrequencies. The model predicts the natural frequencies with an error below 5% for all modes. The shape of the eigenmodes obtained via the FE model are also reported in the figure.

We then compared the axial velocity measured at three target points over the membrane, with that estimated by the FE model (Fig. 4b). We selected three points ($P_1, P_2, P_3$, as schematically indicated in Fig. 4b), of which one ($P_2$) is located on the mean diameter of the DE, whereas the others ($P_1, P_3$) are at a radial distance of approximately 8 mm from the first point. The results in Fig. 4b are relative to a DE membrane biased by $h = 15$ mm, and subject to a sweep excitation with bias of 2 kV and amplitude of 100 V. The plots compare the experimental amplitude of the velocity as a function of the frequency with FE frequency-domain simulations. The damping $\eta_s$ used in the simulation (see Tab. 1) has been calibrated in such a way that the amplitude of the first velocity peak (corresponding to mode $(0, 1)$) matches the experimental data. The model is able to capture the order of magnitude of the measured velocity, even though it fails to replicate the exact trends. In particular, the model predicts a substantial decrease in the velocity of $P_2$, not measured experimentally, in the neighbourhood

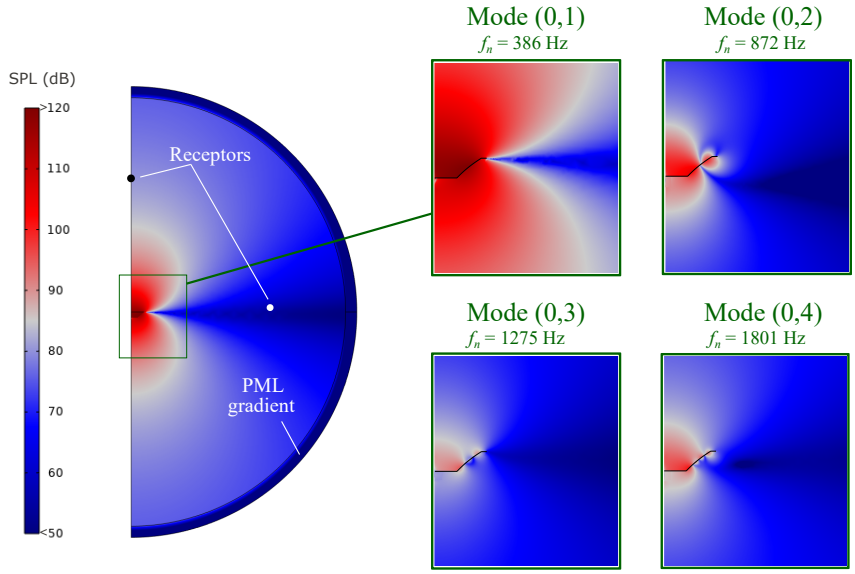


Figure 5: Contour plot of the SPL at the natural frequency of mode $(0, 1)$. The insets represent zoomed views on the field around the DE, at the eigenfrequencies of the different modes. Plots are relative to a scenario with $h = 15$ mm and $V_b = 2$ kV.

of the natural frequency of $(0, 2)$, for which this point behaves as a node. This is possibly due to the complex viscoelastic dynamics of the DE (not accurately described by the model) or inhomogeneities in the membrane, which cause mismatches in the exact position of the nodes or even complex mode behaviours, such as travelling nodes.[25] In addition to that, whereas the model captures the velocity trend (for all points) in correspondence of the first natural frequency (mode $(0, 1)$), it underestimates the amplitude of the peaks corresponding to the other natural frequencies. This is possibly due to an oversimplistic choice of the damping model (Eq. (3)), which does not entirely capture the complex modal behaviour of the DE membrane. This limitation can be possibly overcome by resorting to multi-parameter damping models (e.g., Maxwell viscoelastic model[26]), which however are complex to calibrate and require dedicated experiments, or resorting to a modal formulation, which makes use of modal damping coefficients, which can be calibrated individually.[13]

Although the model is not able to accurately reproduce specific aspects of the DEA dynamics, it still allows capturing the global response and forecasting the order of magnitude of the velocity on the membrane. Therefore, it proves itself able to describe the acoustic response of the system. We used frequency domain simulations to calculate the SPL distribution generated by the DE at different frequencies. Fig. 5 shows a contour plot with the spatial distribution of the SPL at a target frequency (i.e., the eigenfrequency of mode $(0, 1)$), and a close-up view on the pressure field surrounding the DE at different frequencies (close to the relevant eigenfrequencies). The contour plots highlight the function of the PML, which induces an artificial sharp gradient in the sound pressure level at the edge of the domain. Although the pressure field in the immediate neighbourhood of the sample is not entirely representative of the real scenario (because of the presence of additional structural components not included in the model), the plots highlight how the sound radiation patterns vary for different vibration modes. In particular, whereas mode $(0, 1)$ causes the entire membrane surface to move in a single direction, higher order modes (with multiple antinodes) cause multidirectional pumping, which generally leads to a sharper decrease in the SPL in the neighbourhood of the membrane. The membrane has a clear directivity pattern, with little radiation being produced in the directions perpendicular to the membrane's axis.

The acoustic frequency response of the speaker, measured at a receptor point on the axis (0.35 m from the membrane perimeter), is shown in Fig. 6a for a test with $h = 15$ mm and different values of the bias voltage $V_b$. The approximate location of the membrane eigenfrequencies (for the case $V_b = 2kV$) is marked in the plot, for comparison. The acoustic response presents a clear peak (with values over 65 dB for $V_b > 2$ kV) in correspondence of the eigenfrequency of mode $(0, 1)$, whereas the other eigenfrequencies cause smaller variations

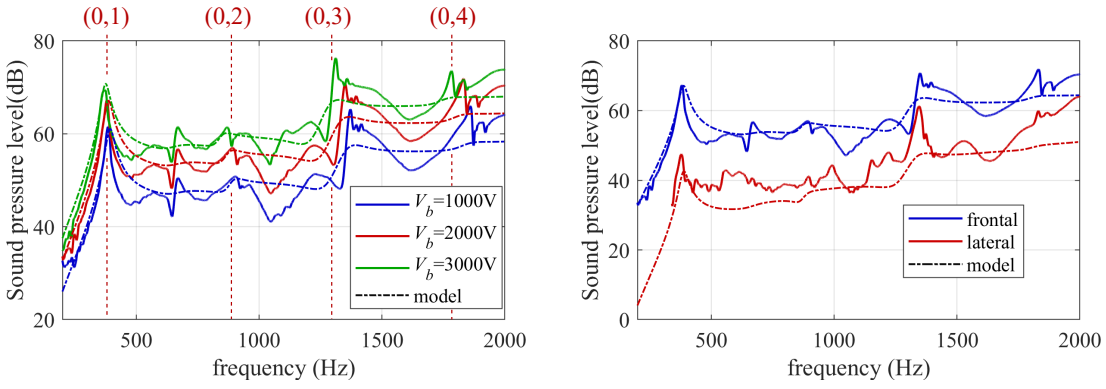


(a) (b)

Figure 6: (a) SPL at a receptor point on the device axis (0.35 m from the membrane), for a pre-load $h = 15$ mm and different values of the bias voltage $V_b$. (b) SPL at two different receptor points (on-axis, and perpendicular to the axis, at 0.35 m from the membrane), for a pre-load $h = 15$ mm and bias voltage $V_b = 2$ kV. The low-frequency portion of the experimental SPL at the lateral receptor point is not reported, as it was too low to be accurately resolved with the available instrumentation. In both plots, continuous lines represent experimental data, whereas dash-dot lines represent model predictions.

in the SPL, as they do not induce a unidirectional deflection of the membrane as in mode $(0, 1)$ (see Fig. 5). Whereas an increase in the average SPL is recognisable at frequencies larger or equal to the eigenfrequency of $(0, 3)$, modes $(0, 2)$ and $(0, 4)$ (i.e., the modes with an even number of antinodes) marginally affect the sound response, as in this case roughly half of the membrane surface pushes the air in a direction, while the other half pumps air in the opposite direction. Increasing the electrical bias causes an increase in the SPL (with differences of up to 7 dB between consecutive voltage values), as it causes a decrease in the DE stiffness (softening effect due to the Maxwell stress) and, hence, an increase in the membrane motion amplitude.[13] The model is able to capture the frequency trend of the SPL and its dependency on the bias voltage. In particular, the model correctly describes the amplitude/shape of the first peak (associated to mode $(0, 1)$), the increase in SPL associated to mode $(0, 3)$, and the average values of the SPL throughout the range. Nonetheless, it is not able to describe specific peaks and localised fluctuations, either because of its rough description of the system damping (see also Fig. 4b) or because of unmodelled effects (e.g., the interactions with the acoustic box walls and the support structure). Fig. 6b shows a comparison between the SPL measured in front of the device (along the axis) or in a perpendicular direction aligned with the DE frame (see also Fig. 5). As observed from the contours in Fig. 5, the SPL on the axis is significantly larger than that measured at 90° (with maximum differences close to 20 dB), hence confirming that the DE membrane under investigation has a strong directional behaviour. The model is able to quantitatively describe the differences between the two scenarios. The SPL trend measured by the lateral receptor is predicted with less accuracy, both because this is more strongly affected by unmodelled effects (e.g., reflections from the structural elements) and because the measurement itself is less accurate in this second case, given the relatively low values of SPL.

In, Fig. 7, we compare the SPL obtained by varying the off-plane displacement $h$, at a constant bias voltage $V_b = 2$ kV. Increasing $h$ within the considered range causes a sensible increase in the natural frequencies, and leads to larger values of the SPL over the entire frequency range (with differences of up to 20 dB between the cases with $h = 10$ mm and $h = 20$ mm). The model is able to effectively capture the quantitative variations of SPL with $h$, and, overall, well predicts the frequency response of the DE diaphragm in the different scenarios.

## 5. CONCLUSION

In this paper, we presented a finite element (FE) model and an experimental characterisation of the vibratory and acoustic behaviour of a dielectric elastomer (DE) membrane subject to high-frequency electrical excitation. DEs are a promising option for the development of coil-free loudspeakers, which use an active polymeric membrane both as an acoustic diaphragm and an actuator, and might lead to extremely compact and lightweight loudspeaker

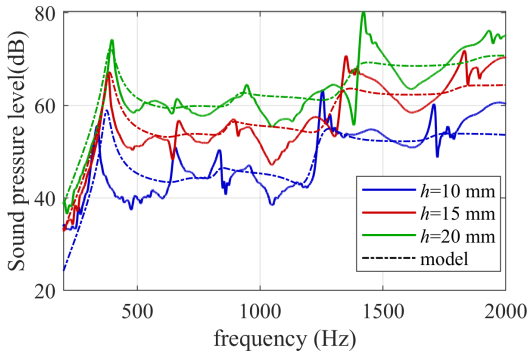


Figure 7: SPL at a receptor point on the device axis (0.35 m from the membrane), for a bias voltage $V_b = 2$ kV and different values of the membrane off-plane displacement $h$. Continuous lines represent experimental data, whereas dash-dot lines represent model predictions.

designs. The complex electro-visco-elastic response of the DE materials makes the design of DE loudspeakers a complex task, and demands for dedicated numerical tools for analysis.

Here, we considered an annular DE membrane deformed out-of-plane in between two fixed frames. We presented a fully-coupled FE model for the system, which combines a hyperelastic model of the membrane mechanical response, an electrostatic coupling contribution that describes the electrical excitation, and an acoustic model of the sound pressure field, which includes the calculation of acoustic loads applied on the membrane. Compared to formulations proposed in the past, the present model entirely relies on a commercial FE software (Comsol Multiphysics), and thus provides an easy-to-replicate framework for design engineers and scientists. We validated the model against experimental measurements of the DE membrane vibrational frequency response (obtained with a laser vibrometer) and the sound pressure level (SPL). We explored the dependency of the frequency response on different parameters (e.g., the mechanical pro-load and the bias voltage). Making use of standard hyperelastic models and a simplified description of damping, the model is able to capture the average qualitative trend of the DE membrane SPL with frequency, and its dependency on the design/control parameters. Limitations to the present work are associated to the simplified damping model used in this work, which limit the extent to which the model matches the experimental data. In the future, this issue might be overcome by resorting to modal formulations and calibrating the modal damping with experiments, or by integrating advanced viscoelastic models able to capture the DE's mechanical dynamics with better accuracy.

## ACKNOWLEDGMENTS

The authors gratefully thank Bettina Fasolt and Tobias Willian (Intelligent Material Systems Lab, Saarland University) who prepared the screen-printed electrode samples.

This project has received funding from the European Union's Horizon 2020 research and innovation programme under the Marie Skłodowska-Curie grant agreement No 893674 (DEtune). The experimental equipment used for the tests was partly sponsored by the ME Saar Foundation, in the framework of the start-up funding of Saarland University.

## REFERENCES

[1] Hajiesmaili, E. and Clarke, D. R., "Dielectric elastomer actuators," *Journal of Applied Physics* **129**(15), 151102 (2021).

[2] Duduta, M., Clarke, D. R., and Wood, R. J., "A high speed soft robot based on dielectric elastomer actuators," in [*2017 IEEE International Conference on Robotics and Automation (ICRA)*], 4346–4351, IEEE (2017).

[3] Henke, E.-F. M., Schlatter, S., and Anderson, I. A., "Soft dielectric elastomer oscillators driving bioinspired robots," *Soft robotics* **4**(4), 353–366 (2017).

[4] Moretti, G., Rosset, S., Vertechy, R., Anderson, I., and Fontana, M., "A review of dielectric elastomer generator systems," *Advanced Intelligent Systems* **2**(10), 2000125 (2020).

[5] Heydt, R., Pelrine, R., Joseph, J., Eckerle, J., and Kornbluh, R., "Acoustical performance of an electrostrictive polymer film loudspeaker," *The Journal of the Acoustical Society of America* **107**(2), 833–839 (2000).

[6] Gareis, M. and Maas, J., "Modal analysis of circular buckling dielectric elastomer transducers," in [*Electroactive Polymer Actuators and Devices (EAPAD) XXIII*], **11587**, 1158722, International Society for Optics and Photonics (2021).

[7] Sugimoto, T., Ando, A., Ono, K., Morita, Y., Hosoda, K., Ishii, D., and Nakamura, K., "A lightweight push-pull acoustic transducer composed of a pair of dielectric elastomer films," *The Journal of the Acoustical Society of America* **134**(5), EL432–EL437 (2013).

[8] Hosoya, N., Baba, S., and Maeda, S., "Hemispherical breathing mode speaker using a dielectric elastomer actuator," *The Journal of the Acoustical Society of America* **138**(4), EL424–EL428 (2015).

[9] Rustighi, E., Kaal, W., Herold, S., and Kubbara, A., "Experimental characterisation of a flat dielectric elastomer loudspeaker," in [*Actuators*], **7**(2), 28, Multidisciplinary Digital Publishing Institute (2018).

[10] Garnell, E., Rouby, C., and Doaré, O., "Dynamics and sound radiation of a dielectric elastomer membrane," *Journal of Sound and Vibration* **459**, 114836 (2019).

[11] Garnell, E., Doaré, O., and Rouby, C., "Coupled vibro-acoustic modeling of a dielectric elastomer loudspeaker," *The Journal of the Acoustical Society of America* **147**(3), 1812–1821 (2020).

[12] Hochradel, K., Rupitsch, S., Sutor, A., Lerch, R., Vu, D., and Steinmann, P., "Dynamic performance of dielectric elastomers utilized as acoustic actuators," *Applied Physics A* **107**(3), 531–538 (2012).

[13] Moretti, G., Rizzello, G., Fontana, M., and Seelecke, S., "High-frequency voltage-driven vibrations in dielectric elastomer membranes," *Mechanical Systems and Signal Processing* **168**, 108677 (2022).

[14] Berselli, G., Vertechy, R., Vassura, G., and Parenti-Castelli, V., "Optimal synthesis of conically shaped dielectric elastomer linear actuators: design methodology and experimental validation," *IEEE/ASME Transactions on Mechatronics* **16**(1), 67–79 (2011).

[15] Rizzello, G., Hodgins, M., Naso, D., York, A., and Seelecke, S., "Modeling of the effects of the electrical dynamics on the electromechanical response of a DEAP circular actuator with a mass–spring load," *Smart Materials and Structures* **24**(9), 094003 (2015).

[16] Moretti, G., Rizzello, G., Fontana, M., and Seelecke, S., "A multi-domain dynamical model for cone-shaped dielectric elastomer loudspeakers," in [*Electroactive Polymer Actuators and Devices (EAPAD) XXIII*], **11587**, 115871K, International Society for Optics and Photonics (2021).

[17] Kinsler, L. E., Frey, A. R., Coppens, A. B., and Sanders, J. V., [*Fundamentals of acoustics*], John Wiley and Sons (1999).

[18] Jabareen, M. and Eisenberger, M., "Free vibrations of non-homogeneous circular and annular membranes," *Journal of Sound and Vibration* **240**(3), 409–429 (2001).

[19] Moretti, G. and Rizzello, G., "A linear parameter-varying modelling approach for dielectric elastomer loudspeakers," in [*10th Vienna International Conference on Mathematical Modelling. In review*], IFAC (2022).

[20] Merriweather, A., "Acoustic radiation impedance of a rigid annular ring vibrating in an infinite rigid baffle," *Journal of Sound and Vibration* **10**(3), 369–379 (1969).

[21] COMSOL Multiphysics, *COMSOL Multiphysics - Reference manual*, 5.5 ed. (2019).

[22] Holzapfel, G. A., [*Nonlinear solid mechanics - A continuun approach for Engineering*], vol. 24, Wiley Chichester (2000).

[23] Suo, Z., "Theory of dielectric elastomers," *Acta Mechanica Solida Sinica* **23**(6), 549–578 (2010).

[24] "Elastosil 2030 films catalogue, Wacker." https://www.wacker.com/h/medias/7091-EN.pdf.

[25] Adhikari, S., "Optimal complex modes and an index of damping non-proportionality," *Mechanical systems and signal processing* **18**(1), 1–27 (2004).

[26] Khan, K. A., Wafai, H., and Sayed, T. E., "A variational constitutive framework for the nonlinear viscoelastic response of a dielectric elastomer," *Computational Mechanics* **52**(2), 345–360 (2013).